Impulsive stimulated Brillouin scattering studies of the ferroelectric phase transition in tris-sarcosine calcium chloride

Lap-Tak Cheng and Keith A. Nelson
Department of Chemistry, Massachusetts Institute of Technology, Cambridge, Massachusetts 02139
(Received 11 October 1988)

The longitudinal acoustic-phonon anomalies along all three principal axes of tris-sarcosine calcium chloride near its ferroelectric phase transition were studied using "impulsive" stimulated Brillouin scattering with scattering angles of 23.78° and 6.03°. Logarithmic corrections to mean-field behavior are observed in both phases. Dynamic dispersion analysis of ultrasonic, Brillouin scattering, and the present results confirmed Landau-Khalatnikov order-parameter dynamics with an elementary relaxation time $\tau_0 = 5.5 \times 10^{-12}$ s K. The unusual acoustic behavior along the polar axis is determined to result from a weak depolarization field and the proximity to a tricritical point. Energy relaxation is believed to be the source of sharp acoustic anomalies along the polar axis which are observed in ultrasonic studies but not in optical experiments which probe higher acoustic frequencies.

I. INTRODUCTION

The ferroelectric phase transition of tris-sarcosine calcium chloride (TSCC), $(CH_3NHCH_2COOH)_3CaCl_2$, has been the subject of numerous investigations in the past decade. Crystalline TSCC changes from a paraelectric pseudotrigonal structure of $D_{2h}^{16}(Pnmma)$ symmetry to a uniaxial ferroelectric $C_{2v}^{9}(Pna21)$ structure upon cooling near 130 K.[1] The planar sarcosine units exist in two crystallographically inequivalent forms and their librational displacements and internal distortions give rise to a permanent dipole moment along [010] direction in the ferroelectric phase. An extensive hydrogen-bonding network connects the sarcosine molecules to the $CaCl_2$ lattice. There are three inequivalent hydrogen bonds involving asymmetric N-H-Cl potential wells with different bond lengths. Deuteration studies[2] indicate that the hydrogen bonds do not participate strongly in the phase transition.

The main issues surrounding the TSCC structural phase transition can be grouped into two categories. The first concerns questions of whether the phase transition is predominantly order-disorder or displacive. On one hand, the relatively low-transition temperature, the existence of the hydrogen-bonding network, large transition entropy, dielectric dispersion,[3] and conclusions from detailed Raman and ir spectroscopic analyses[4] all point to an order-disorder phase transition in which the order parameter would be expected to show relaxational (i.e., Debye) dynamics. On the other hand, the observation of underdamped Raman-active soft optic phonon modes[5] represents strong evidence for a displacive transition. In recent years, it has been recognized that strict order-disorder or displacive classification is not valid for most continuous phase transitions. The distinction is often blurred by coupling between relaxation and oscillatory degrees of freedom. In addition, decreasing frequency and increasing damping rate drive most soft modes overdamped near T_c, and few experimental measurements can distinguish between overdamped and relaxational dynamics. In TSCC, recent dielectric measurements up to the GHz regime confirmed that mixing between Debye and oscillatory degrees of freedom does play an important role.[6] The displacive (soft-optic phonon) mode is associated with the sarcosine librations and distortions that appear in the low-temperature phase. It has been suggested that the coupled degree of freedom may be associated with the same molecular motions, but with hopping between different free-energy minima rather than infinitesimal displacements.

A second concentration of interest concerns the critical behavior of the ferroelectric phase transition. A combination of properties makes TSCC a particularly rich testing ground for modern theories of structural phase transitions. First, TSCC is a uniaxial ferroelectric without ferroelasticity in the low-temperature phase. This makes it a prime candidate for observation of logarithmic corrections to mean-field behavior as predicted by Larkin-Khmel'nitskii (LK) theory[7] and subsequent renormalization-group calculations.[8] Mean-field theory breaks down as a result of the anisotropic nature of the dipolar interaction which quenches polarization fluctuations along the ferroelectric (polar) axis but not in other directions. Logarithmic corrections have indeed been observed in dielectric,[9] acoustic,[10] and specific-heat[11] anomalies in TSCC, making it one of the few materials in which dipolar critical behavior has been clearly demonstrated. Second, much evidence exists pointing to an unusually weak dipole moment associated with the polar soft mode. The anomalously small Curie constant (40 to 60 K^{-1}) (Ref. 3) and the weak longitudinal-optic and transverse-optic splitting[12,13] indicate that both short-range and dipolar forces are important in the phase transition. A crossover between dipolar to Ising universality classes is expected at some intermediate temperature

from T_c. Such a crossover has been reported in acoustic[10] and specific-heat[11] studies. Third, along the polar axis, polarization fluctuations are quenched by the presence of a depolarization field. Therefore, no acoustic anomalies are expected along this axis. In TSCC, however, large acoustic anomalies along the polar axis have been observed at both ultrasonic and Brillouin-scattering frequencies. The origin of these anomalies remains in question.

Since electrostrictive coupling between non-symmetry-breaking acoustic strains and the order parameter is always allowed, studies of acoustic anomalies have long been an effective method to investigate structural transitions. In TSCC, ultrasonic measurements at 20 MHz revealed sharp anomalies in longitudinal strains propagating either parallel or perpendicular to the polar axis.[14] Brillouin-scattering experiments at 20 GHz, however, have revealed strong anisotropy, with sharp anomalies along the nonpolar axes and a very gradual temperature dependence in the acoustic behavior along the polar axis.[10,15] Although various explanations have been put forward to account for the differences between ultrasonic and Brillouin-scattering results, direct experimental investigation at intermediate frequencies is needed to clarify the dispersive behavior and its origin.

Until recently, the frequency region between 100 MHz and 10 GHz has been largely inaccessible by conventional techniques. Ultrasonic techniques become difficult due to the thin transducer and sample dimensions involved, and due to strong acoustic attenuation at high frequencies which frustrates the commonly used echo technique. Brillouin-scattering experiments with small scattering angles are extremely difficult as a result of parasitic scattering which swamps the low-frequency region of the spectrum. Recent efforts in performing small-angle scattering in TSCC have been sucessful, but the data collected are rather poor in quality and are not suited for quantitative analysis.[16] In the past few years, an alternative time-domain light scattering method has been developed. It is now possible to obtain accurate acoustic measurements in the 10 MHz–10 GHz region,[17,18] bridging the gap between ultrasonics and frequency-domain Brillouin scattering. Through "impulsive" stimulated Brillouin scattering (ISBS), coherent acoustic phonons of selected polarization, wavelength, and orientation are excited optically with picosecond light pulses, and their time-dependent oscillations and decay are monitored directly in the time domain. ISBS has been used to study acoustic anomalies in the ferroelectric phase transitions of the KDP family crystals.[17] As a result of piezoelectric coupling in the symmetric phase of these crystals, dramatic softening of shear acoustic phonons occurs. The effective photoelastic constant, and hence the signal intensity in an ISBS experiment, also diverges near T_c. The detailed temperature dependences and dispersions of the acoustic anomalies are easily characterized to within several mK of the transition temperature. In TSCC, due to the lack of piezoelectric coupling in the symmetric phase, the acoustic anomalies are only in the few percent range and the signal intensity in an ISBS experiment remains essentially constant throughout the entire temperature range. Therefore ISBS investigations in quadratically coupled systems are more difficult.

In this paper, we report ISBS results from TSCC at temperatures between 300 and 100 K with the transition temperature determined at $T_c = 130.1 \pm 0.2$ K. This represents the first application of ISBS to the study of acoustic anomalies in an electrostrictively coupled system. The longitudinal acoustic velocities along all three principle axes have been measured with two different scattering angles, probing frequencies of about 2 and 0.3 GHz. Together with published ultrasonic[14] and Brillouin-scattering[10,15] results, nearly four decades of acoustic data are assembled. Based on the analysis of these data, we address some of the issues concerning the static and dynamic critical properties of TSCC mentioned earlier. From the ISBS data, dipolar behavior in TSCC is established by the observation of logarithmic corrections in both phases. This result confirms earlier observations of Brillouin backscattering experiments.[10] Using quantitative data on the logarithmic corrections in both phases, we have compared our results with the fluctuational theory of Nattermann.[19] The gradual temperature dependence of the acoustic anomalies along the polar axis observed in Brillouin-scattering experiments is also observed in the ISBS experiments despite the much lower frequencies involved. Its origin, as first suggested by Smolensky *et al.*,[10] is confirmed by dispersion analyses to be a result of a weak depolarization field and the proximity of the transition to a tricritical point. The dynamics of the transition agree well with a Debye model in which the order parameter relaxation time shows a Landau-Khalatnikov temperature dependence with an unusually fast elementary relaxation time $\tau_0 = 5.5 \pm 0.2 \times 10^{-12}$ s K.

In the next section, the experimental details of the ISBS experiment are described. Section III presents ISBS data on longitudinal acoustic waves in TSCC and highlights various time-dependent and temperature-dependent features in the data. In Sec. IV the mean-field and fluctuational theories for quadratically coupled acoustic anomalies in a uniaxial ferroelectric transition are reviewed and their predictions compared to current results. Mean-field theory is first discussed to establish the background behavior from which logarithmic corrections can be extracted from the data. The depolarization field along the polar axis is emphasized in order to understand the observed acoustic anisotropy. Finally, acoustic behavior in different frequency regimes is discussed in terms of order-parameter and energy relaxation dynamics. Section V summarizes the essential conclusions of this work.

II. EXPERIMENT

A. Time-domain light scattering experiments

The ISBS experiment is illustrated schematically in Fig. 1. Two parallel-polarized picosecond laser pulses derived from the same laser, of central frequency and wave vectors $(\omega_L, \mathbf{k}_1)$ and $(\omega_L, \mathbf{k}_2)$, are overlapped spatially and temporally inside a sample to excite coherent acoustic phonons of frequency and (difference) wave vectors

$(\omega_a, \pm\mathbf{q}_0)$, where $\mathbf{q}_0=\mathbf{k}_1-\mathbf{k}_2$ and $\omega_a/|q_0|=v_a(q_0)$, with v_a the acoustic velocity. The excitation pulse duration must be short compared to a single acoustic oscillation cycle for effective phonon generation to occur. The optical field of the interfering pulses exerts a spatially periodic and temporally impulsive electrostrictive force on the acoustic modes through stimulated Brillouin scattering. This force drives an acoustic standing wave (two counterpropagating waves) whose wavelength and orientation match those of the optical interference pattern, i.e., with wave vectors $\pm\mathbf{q}_0$. If weak optical absorption occurs, longitudinal acoustic waves can also be launched through sudden heating and subsequent thermal expansion.

At early times after excitation, before substantial acoustic propagation takes place, the two traveling acoustic waves interfere and constitute a standing wave inside the excitation volume. In the absence of absorption, the acoustic strain S can be described by[20]

$$S(\mathbf{q},t)\propto\frac{p}{\omega_a}e^{-\gamma_a t}\sin(\omega_a t)\delta(\mathbf{q}\pm\mathbf{q}_0)\ , \tag{1}$$

where p is the appropriate photoelastic constant, and ω_a and γ_a are the acoustic frequency and attenuation, respectively. When laser heating occurs, an additional term must be added representing thermal expansion due to the periodic temperature profile. The total strain due to ISBS and heating is[20]

$$S(\mathbf{q},t)\propto\{A_1[1-e^{-\gamma_a t}\cos(\omega_a t)] + A_2 e^{-\gamma_a t}\sin(\omega_a t)\}\delta(\mathbf{q}\pm\mathbf{q}_0)\ , \tag{2}$$

where A_1 and A_2 are relative amplitudes. Thermal diffusion has been neglected in the first term of Eq. (2).

The spatially periodic standing wave modulates the refractive index of the material, giving rise to a time-dependent volume "grating" which can coherently scatter or "diffract" a variably delayed probe pulse incident at the phase-matching angle for Bragg diffraction (see Fig. 1). The diffracted probe pulse remains polarized when scattered by a longitudinal wave. The intensity I of the diffracted light, i.e., the grating's diffraction efficiency, depends quadratically on the extent of acoustic displacement. As the acoustic standing wave oscillates, the diffracted probe intensity oscillates between zero and its maximum values. Therefore, by monitoring the time-dependent diffracted intensity, the coherent acoustic oscillations and decay can be monitored in the time domain. Equation (1) shows that for stimulated Brillouin-scattering excitation, the standing wave displacement vanishes twice during each acoustic cycle. Therefore, the diffracted probe intensity,

$$I\propto S^2\propto\frac{1}{\omega_a}[e^{-\gamma_a t}\sin(\omega_a t)]^2\ , \tag{3}$$

also vanishes twice each acoustic cycle. The behavior is slightly more complicated when heating also occurs and the strain is described by Eq. (2).

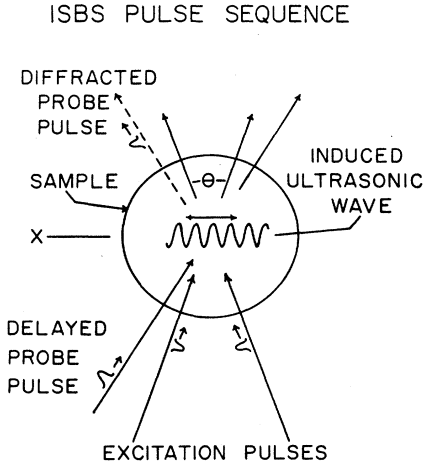

FIG. 1. Schematic diagram of the ISBS experiment. The crossed excitation pulses "impulsively" excite an ultrasonic standing wave in the sample. The standing wave modulates the refractive index of the material and so can be detected by Bragg diffraction of variably delayed probe pulses. The time-dependent oscillations and decay of diffracted signal yield the acoustic frequency and attenuation rate.

B. Experimental setup

The ISBS experimental setup, illustrated in Fig. 2, has been described previously.[17] The light source is a Q-switched and mode-locked Nd:YAG laser operating at a 500-Hz repetition rate to produce 85-ps pulses with up to 80 μJ of energy. Two single pulses are isolated with electro-optic Pockels' cells for ISBS excitation. A third single pulse is isolated, frequency doubled, variably delayed, and used to probe the coherent acoustic wave at the Bragg angle. Noise rejection is accomplished by using lock-in amplification. The optical delay line is double passed to provide a maximum delay of about 20 ns. Longer delays (up to several hundred ns) have been achieved in other experiments by using different single pulses for the probe.[18]

Seeds of TSCC were obtained by slow evaporation of aqueous solutions containing the stoichiometric ratio of sarcosine and $CaCl_2$. Due to the pseudotrigonal struc-

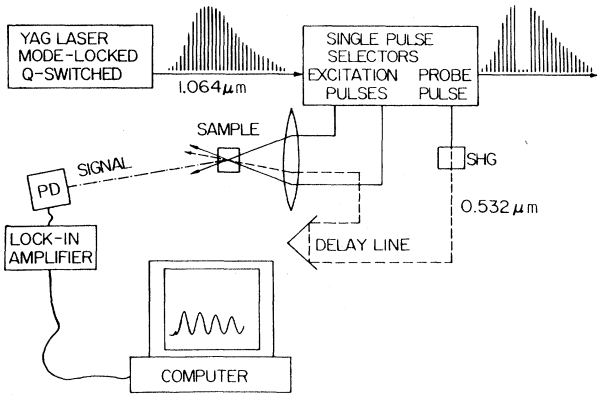

FIG. 2. Schematic diagram of the ISBS experimental setup. See text for details. SHG = second harmonic generator; PD = photodiode.

ture, seeds obtained from spontaneous nucleation are invariably twinned. Single-domain portions are cut and planted in a solution with excess sarcosine. Subsequent growth by slow evaporation and gentle stirring yielded large, high-quality single-domain crystals. From a single large crystal, two samples with dimensions $5\times5\times3$ mm were cut. Appropriate surfaces were polished on a soft surface (nylon or paper) with alumina powder down to 0.3 μm to allow optical access to all three principle axes. The crystal orientations were confirmed by x-ray crystallography. The samples were housed inside aluminum cells with optical windows. Isopentene served as partial index matching fluid and provided even thermal contact. The sample temperature was monitored with calibrated Si diodes mounted directly on the aluminum cell in close proximity to the crystal. A Palm Beach Cryosystem controller (model 4075) regulated the sample temperature. Temperature stability within 5 mK was obtained for periods up to 20 min.

The ISBS experiments were carried out with parallel (vertically relative to the scattering plane) polarized excitation and probe pulses. The fundamental of the Nd:YAG laser served as excitation radiation. To time resolve the oscillations of high-frequency longitudinal waves, a shorter probe provided by a synchronously pumped dye laser was used. Considerable care was taken in arranging the scattering geometry. It is well known that due to depolarization field effects, alignment of the acoustic wave vector on or off the basal plane will result in strong anisotropy of the acoustic anomalies observed. Alignment of the scattering wave vector was guided by the surface reflection of the samples, and fine adjustments were made to eliminate beating patterns in ISBS signal resulting from excitation of quasilongitudinal and quasitransverse waves along nonpure mode directions. In order to determine the acoustic velocities accurately, the scattering angles were measured carefully using a rotational stage from Klinger which has a 2-min relative accuracy. The experiments reported in this paper were performed with scattering angles (θ) of 23.78° and 6.03°. The uncertainty in measurement of the smaller angle was $\pm0.5\%$. Note that "scattering angle" is defined here as the angle between the excitation pulses. The wave vector in the 6.03° experiments is the same as that which would result from a scattering angle of about 2° in a spontaneous light scattering experiment with 514.5 nm light.

Another geometric consideration concerns the finite laser spot sizes in the excitation region. As the two traveling acoustic waves propagate out of the excitation region, the diffracted intensity of the probe pulse shows an artificial decay. This decay is completely determined by the excitation and probe spot sizes and speed of sound in the material, and its detailed time dependence has been derived.[21] To minimize this effect, cylindrical focusing is often used when signal level and sample quality permit. Due to the poor quality of the TSCC crystal surfaces, small spot sizes (≈200 μm) were required to maintain good signal-to-noise ratios in the data. Therefore the "runoff" effects in the data were taken into account as an instrumental function whose analytical form is known. At the 6.03° scattering geometry, the intrinsic acoustic attentuation rate is low and the run-off artifacts prevented determination of acoustic attenuation rates. Only velocity values were obtained.

Time-domain and frequency-domain procedures have been adopted for data analysis, and both yielded essentially identical values for acoustic frequencies and attentuation rates. The former utilizes curve-fitting routines based on the Marquardt-Levenberg algorithm[22] to fit the time-domain data directly. The proper response function, which accounts for finite spot-size effects, was used and yielded excellent fits to the data. The latter procedure performs Fourier transforms of the data into the frequency domain. The acoustic parameters were obtained by fits with Lorentzian profiles. Results presented here were obtained with the time-domain procedure.

III. EXPERIMENTAL RESULTS

Figures 3 and 4 show ISBS data from longitudinal acoustic waves taken with scattering angles of 23.78° and 6.03°, respectively, and with wave vectors along the a axis of TSCC. From Eq. (3), it is apparent that ISBS signal oscillates at twice the acoustic frequency ($2\omega_a$) and decays at twice the attenuation rate. The effect of laser heating, apparent from the square of Eq. (2), is to add to the signal a frequency component at ω_a, leading to signal maxima of alternating amplitudes. Also apparent is the Gaussian taper of the oscillatory signal and the Gaussian rise of a nonoscillatory signal at the baseline at long times. These effects are due to runoff of the acoustic waves as discussed above. Note that the data in Fig. 3 are due primarily to stimulated Brillouin-scattering excitation (hence the $2\omega_a$ oscillation frequency) while the data in Fig. 4, recorded with a smaller scattering angle, are due mainly to heating (oscillation at frequency ω_a). This is because the stimulated scattering contribution to the signal decreases as $1/\omega_a^2$ [see Eq. (3)]. A comparison of the data scans taken at different temperatures clearly shows that the velocity anomalies at both scattering angles are readily measured. The anomalous increase of acoustic attenuation is also easily observed in the high-frequency experiment.

To facilitate dispersion analysis over a wide frequency range, existing high-quality ultrasonic,[14] right-angle Brillouin-scattering,[15] and back Brillouin-scattering[10] results were taken from the literature. Together with the ISBS data, analysis over four decades of frequency was carried out. Due to the scatter of reported velocity and transition-temperature values, each data set was normalized against its reported value at 50 K above T_c and its temperature axis translated to obtain a uniform transition temperature at the present measured value. The discrepancies in velocity values most likely result from uncertainty in scattering angle measurements among the light scattering data. The ISBS values agree well ($\approx1\%$) with ultrasonic values along the a and c axes but differ by 6% along the polar axis. Rather erratic dispersion far from the transition temperature has been reported[16] between 2 and 30 GHz along the c and b axes. Careful ISBS measurements at room temperature between 0.3 and 4 GHz along all three principle axes have not re-

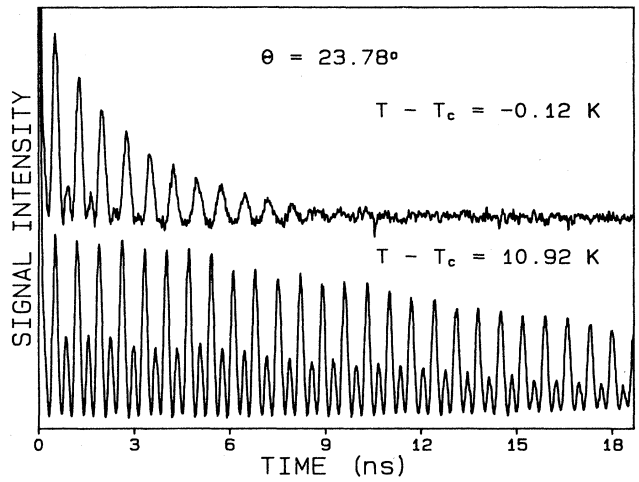

FIG. 3. ISBS data from longitudinal acoustic mode along a axis of TSCC ($\theta=23.78°$). Longitudinal acoustic data shown were obtained with V-V polarized excitation pulses. The alternating maximum intensities were caused by a weak laser-heating contribution to the ISBS signal. The top trace was taken near the transition temperature, showing the anomalous increase in acoustic attenuation. The small change in acoustic frequency is clearly measurable. Due to the small excitation spot sizes used, acoustic propagation leads to a gradual Gaussian taper of the intensity maxima and a Gaussian rise of the baseline at long times.

vealed any dispersion, as can be seen in Fig. 5. Acoustic velocities at room temperature are $v_a=3.72$, $v_b=4.99$, and $v_c=4.65$ km/sec.

The anomalous changes in acoustic velocities along the principle axes, measured with both scattering angles, are presented in Fig. 6. The velocity values were calculated from the measured frequencies and scattering angles according to

$$v_a=\frac{\omega_a\lambda_L}{2\sin(\theta/2)},$$

where $\lambda_L=1.06$ μm and θ is the scattering angle. Note that the refractive index and therefore its temperature dependence does not enter into the determination of acoustic velocity. No thermal hysteresis was detected as the phase transition was approached from above or below, indicating an essentially continuous transition. Along the a and c axes, very sharp decreases of the velocities were observed as temperature was reduced near T_c. The decrease occurred within a range of 100 mK from the maximum slope to the minimum velocity. A rather rapid rise followed in the low-temperature phase, recovering over 50% of the anomaly within 20 K. The velocity anomaly along the b axis, however, displayed markedly different behavior. The drop was stretched out for nearly 5 K. Also evident is the gradual decrease near T_c in the high-temperature phase. Along the a and b axes, experiments performed with two scattering angles yielded virtually identical results. This indicates that the frequency range accessed by the ISBS experiments is well within the low-frequency limit in which $\omega_a\tau\ll 1$, where τ is the order parameter relaxation time.

Figure 7 shows the acoustic attenuation anomalies plotted together with the velocities to illustrate their relative temperature dependences. The attenuations along the a and c axes remain below the instrumental capability for measurement throughout the high-temperature (HT) phase and abruptly rise and fall through a maximum at a temperature T_m. The rise with decreasing temperature is much sharper than the subsequent fall, displaying a λ-type peak with half width $\Delta T\approx 0.1$ K. Along the b axis, however, no anomalous increase was observed. For the 6.03° scattering angle experiment, acoustic attenuation along any direction remained below the instrumental limit throughout the entire temperature range studied.

From T_m and ΔT, assuming Debye relaxational dy-

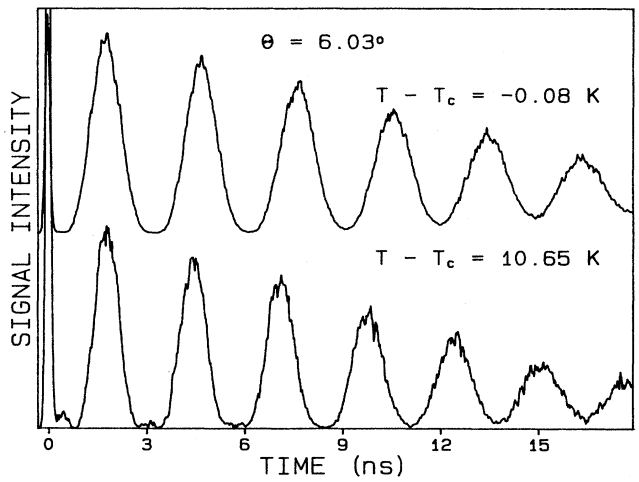

FIG. 4. ISBS data from longitudinal acoustic mode along a axis of TSCC ($\theta=6.03°$). At small wave vectors, the signal is dominated by the laser-heating contribution. Although acoustic attenuation is too weak to be measured accurately, the velocity anomaly is determined.

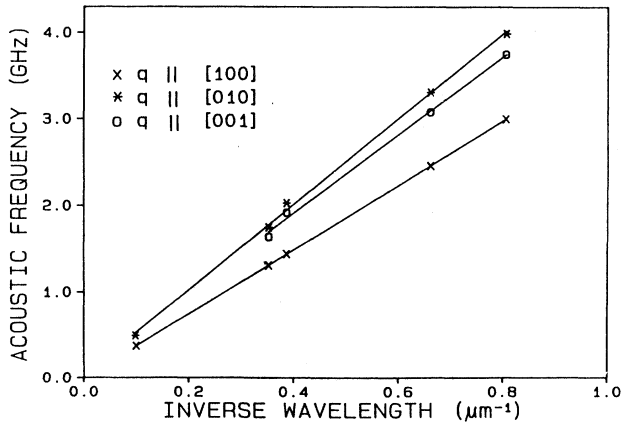

FIG. 5. Room-temperature frequency dispersion in TSCC. Longitudinal acoustic frequencies measured at room temperature with different wave vectors are shown for the principle axes. Linear dispersion is evident in each case, indicating no dispersion in the room-temperature velocities.

namics for the order parameter with a Landau-Khalatnikov temperature dependence for the relaxation time $\tau=\tau_0/(T_c-T)$, the transition temperature is determined, in the low-frequency limit, by[10]

$$T_c=T_m+\frac{\Delta T}{2\sqrt{3}} . \tag{4}$$

Based on the 23.78° scattering angle data, the transition temperature is determined to be $T_c=130.21$ K with absolute uncertainty of ±0.2 K. Relative temperature measurements are good to within ±0.01 K. This value of T_c agrees well with that of calorimetric studies.[11] Since the velocity anomalies are only a few percent of the background values, it is valid to assume that $\omega_a\tau=1$ occurs at the midpoint of the velocity anomalies. The calculated elementary relaxation time, $\tau_0=5.5\pm0.2\times10^{-12}$, agrees well with those determined by Brillouin scattering.[15]

IV. DISCUSSION

In this section we attempt to explain our results and those of others in terms of a consistent theoretical framework. We begin by reviewing mean-field predictions for

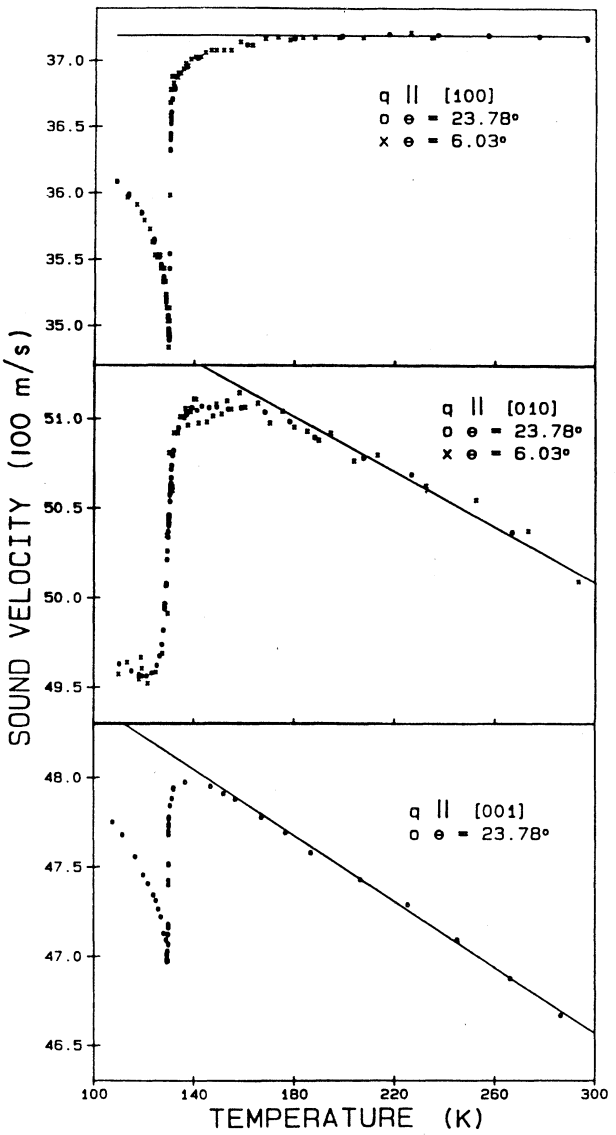

FIG. 6. Longitudinal acoustic velocity anomalies along principle axes of TSCC. Acoustic velocities were determined according to the measured frequency and scattering geometry. Along the *a* and *b* axes, data obtained with two scattering angles are shown. Note the sharp anomalies along the *a* and *c* axes in comparison to the gradual behavior along the polar *b* axis. The solid lines define the background changes.

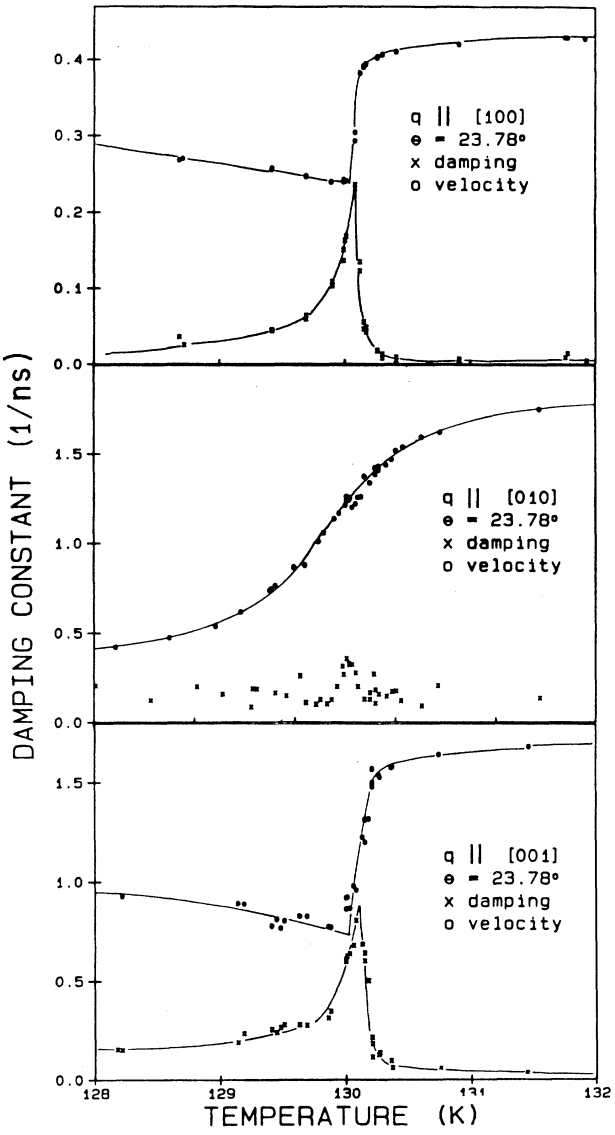

FIG. 7. Longitudinal acoustic attenuation anomalies along principle axes of TSCC. Acoustic attenuation values shown were obtained directly from best fits of ISBS data. The corresponding velocities are also shown on the expanded temperature scale. Note the sharp attenuation features along the *a* and *c* axes and the lack of clearly anomalous behavior along the polar *b* axis. Solid lines are only guides to the eye.

the behavior of acoustic phonons quadratically coupled to the order parameter. Proximity to a tricritical point is accounted for. Next, the depolarization field and its effects on the acoustic modes are treated. Logarithmic corrections to mean-field behavior are then included. Finally, acoustic dispersion due to order-parameter dynamics is accounted for. At each step in the discussion, the theoretical predictions are compared to experimental results.

A. Mean-field behavior

The familiar Landau expansion[23] of the free-energy density (Φ), accounting for quadratic coupling between order parameter, the uniaxial polarization P, and all longitudinal strains S_i along crystallographic axes $i=1$, 2, or 3 is

$$\Phi(p,T,P,S_i)=\Phi_0+\frac{A}{2}P^2+\frac{B}{4}P^4+\frac{C}{6}P^6 + \frac{C_{ii}^P}{2}S_i^2+\frac{Q}{2}P^2S_i+\cdots , \quad (5)$$

where A, B, and C are expansion coefficients with $A=A_0(T-T_c)$ the only temperature-dependent quantity. C_{ii}^P represents the longitudinal elastic constant along the i direction, and Q the electrostrictive coefficient which couples P and S_i. The sixth-order term has been included because the ferroelectric transition in TSCC is known to be in close proximity to a tricritical point, i.e., $B^2<4AC$. For brevity, no gradient terms have been included.

Minimizations of the thermodynamic potential give the following expression for the equilibrium values of the longitudinal strains and order parameter in the low-temperature (LT) phase:

$$S_i=-\frac{Q}{2C_{ii}^P}P^2 , \quad (6)$$

$$P^2=-\frac{B'}{2C}+\left[\frac{A_0}{C}(T_n-T)\right]^{1/2} , \quad (7)$$

where

$$B'=B-\frac{Q^2}{2C_{ii}^P} , \quad (8)$$

$$T_n=T_c+\frac{B'^2}{4A_0C} . \quad (9)$$

The transition temperature is unchanged as a result of the quadratic coupling, with spontaneous acoustic strain and polarization vanishing at $T\geq T_c$. The equilibrium polarization susceptibility is, in the LT phase,

$$\chi_0=\left[\frac{\partial^2\Phi}{\partial P^2}\right]^{-1}=\frac{1}{P^2(2B+4CP^2)} . \quad (10)$$

The acoustic anomalies at constant (zero) electric field are given by

$$\Delta C_{ii}^{E=0}=C_{ii}^{E=0}-C_{ii}^P=-4QP^2\chi_0 , \quad (11)$$

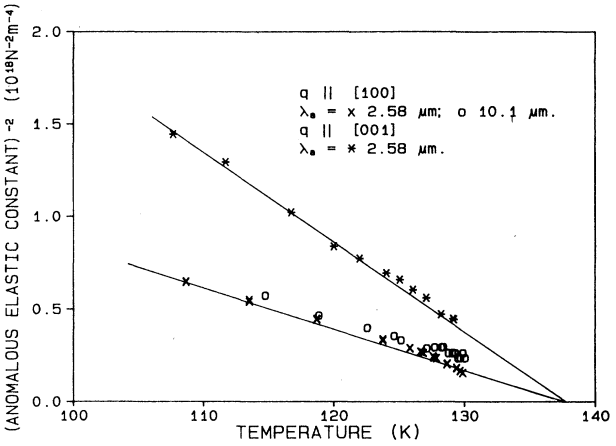

FIG. 8. Low-temperature phase anomalous elastic constants in TSCC. The inverse square-root behavior of the anomalous elastic constants in the LT phase is shown for the a and c axes. The anomalous elastic constants were obtained by subtracting the background values shown by solid lines in Fig. 6. Results from two scattering angles are shown for the a axis. The linear plots for both axes share a common intercept, yielding $T_n=8.9$ K.

where the effective elastic constant at constant (zero) electric field $C_{ii}^{E=0}$ is derived according to the following relation connecting thermodynamic susceptibilities at constant field and at constant conjugate variable:[24]

$$\left[\frac{\partial^2\Phi}{\partial S_i^2}\right]_{E=0}=\left[\frac{\partial^2\Phi}{\partial S_i^2}\right]_P-\frac{(\partial\Phi/\partial P\partial S_i)^2}{(\partial^2\Phi/\partial P^2)_{S_i}} . \quad (12)$$

Since the susceptibility is independent of P in the HT phase, mean-field theory predicts no anomalous acoustic behavior for $T>T_c$ where the equilibrium value of the order parameter is zero by definition. For $T\leq T_c$, substituting Eqs. (7) and (10) into Eq. (11) gives

$$\Delta C_{ii}^{E=0}=\frac{-Q^2}{\sqrt{A_0C}}(T_n-T)^{-1/2}, \quad T\leq T_c . \quad (13)$$

Equation (13) predicts a discontinuous drop in the elastic constant at T_c with a subsequent inverse square rise in the LT phase. Along the a and c axes, such a description for the LT phase agrees well with our observation. Figure 8 is a plot of the inverse square of the anomalous elastic constants versus temperature for the a and c axes. Linear variations are found for both axes with a common intercept giving $T_n-T_c=8.9\pm0.5$ K. T_n provides a measure of the tricritical character of the phase transition. At a tricritical point, $T_n=T_c$. For TGS (triglycine sulfate) in which the sixth-order term in Eq. (5) is known to be unimportant, i.e., far from tricriticality, $T_n-T_c\approx300$ K.[14] In Fig. 8 noticeable deviations from linear behavior occur close to T_c. These deviations are caused by critical fluctuations.

B. Depolarization field

For a uniaxial ferroelectric in which electric polarization is the order parameter, additional consideration is

needed concerning the electric field induced by the spontaneous polarization. From electrostatics, it is well known[25] that an inhomogeneous distribution of electric polarization gives rise to an anisotropic electric field known as the depolarization field $\mathbf{E}_P$. It has the following wave vector dependence:

$$\mathbf{E}_P(\mathbf{q})=\frac{-4\pi[\mathbf{q}\cdot\mathbf{P}(\mathbf{q})]\mathbf{q}}{\epsilon_0 q^2}\ , \tag{14}$$

where ϵ_0 is the background dielectric constant. The presence of $\mathbf{E}_P(\mathbf{q})$ leads to a change of the thermodynamic potential which must be added to Eq. (5). For a fixed wave vector $\mathbf{q}$ along an arbitrary direction, the depolarization field contribution becomes

$$-\mathbf{E}_P(\mathbf{q})\cdot\mathbf{P}(-\mathbf{q})=4\pi q_2^2 P^2/\epsilon_0 q^2\ , \tag{15}$$

where the right-hand side has been simplified for TSCC in which the maginitude of $\mathbf{P}$ fluctuates but the direction is always along the polar (b) axis, i.e., $P_1=P_3=0$. Notice that its effect is highly anisotropic and vanishes only in directions orthogonal to the polarization axis. Along the polar direction, the effect remains even in the limit of q going to zero. Clearly, the inhomogeneous fluctuating properties given by $[\chi(\mathbf{q})]^{-1}$ become highly anisotropic,

$$[\chi(\mathbf{q})]^{-1}=\chi_0^{-1}+\frac{4\pi}{\epsilon_0}\left[\frac{q_2^2}{q^2}\right]\ . \tag{16}$$

In experiments performed with high-frequency acoustic waves, due to the finite wave vectors involved, acoustic anomalies in the low-temperature phase predicted by Eq. (13) are modified by the depolarization field effects. On the plane orthogonal to the polar axis, these effects vanish and Eq. (13) remains unchanged. Off the orthogonal plane, χ_0 in Eq. (11) must be replaced by $\chi(\mathbf{q})$ and the presence of the temperature-independent term in Eq. (16) prevents the divergence of the inhomogeneous polarization susceptibility. This leads to suppression of the corresponding polarization fluctuations. Therefore acoustic anomalies along the polar axis (the b axis of TSCC) are expected to be suppressed. Accounting for the depolarization field, in the limit of tricriticality, the following expression is reached for the temperature dependence of the elastic constant for longitudinal strain along the polar axis:[10]

$$\Delta C_{22}^{E=0}\approx\frac{\sqrt{T_n-T}}{T_n+\dfrac{4\pi}{A_0\epsilon_{22}}-T}\ . \tag{17}$$

This form fits the LT phase data well, as can be seen in Fig. 12 (top half). The constant term appearing in the denominator of Eq. (17) represents the suppression of the acoustic anomaly due to the depolarization field. For TGS, which has a Curie constant $1/A_0=323$ K,[26] this term leads to the complete elimination of the acoustic anomaly along the polar axis. For TSCC, which has an unusually small Curie constant of 40 K, the suppression near T_c results in the rounding of all the sharp features seen along the a and c axes. The anomaly is spread out over a wide (several degree) temperature range. The magnitude of the anomaly is still significant.

C. Logarithmic corrections

Mean-field theory is accurate for systems in which the order parameter interacts through long-range forces. For uniaxial ferroelectrics, due to the anisotropic nature of the dipolar interaction, the dipolar forces are not truly long range. This has been illustrated most convincingly by comparing the Fourier components of the dipolar force in wave-vector space with those of the isotropic long-range force.[27] While the isotropic case has a diverging curvature at the origin in wave-vector space, the anisotropic dipole force does not. As a result, fluctuation effects are not completely suppressed and corrections to mean-field behavior are expected for uniaxial ferroelectrics such as TSCC. Note that if the polarization is piezoelectrically coupled to a soft elastic strain, as in the case of the KDP family crystals, the long-range elastic interactions lead to complete suppression of fluctuation effects.[8]

First-order corrections to mean-field behavior can be calculated by considering higher-order correlations of fluctuations[28] that have been ignored in Eq. (5). Larkin and Khmel'nitskii[7] solved exactly the problem of asymptotic critical behavior in uniaxial ferroelectrics, and found deviations from mean-field results by logarithmic factors. This result has been extended byNattermann[19] to the whole critical region, and his results will be quoted here. The singular part of the free-energy density in the limit of small corrections was found to be

$$\begin{aligned}\Phi_{\text{sing}}=&\tfrac{1}{2}At(1+3b\ \ln a\chi)^{-1/3}P^2\\&+\tfrac{1}{4}B(1+3b\ \ln a\chi)^{-1}P^4\\&-\tfrac{1}{6}T_c\Delta C_0 t^2[(1+3b\ \ln a\chi)^{1/3}-1]\ ,\end{aligned} \tag{18}$$

where $t=(T-T_c)/T_c$, b and a are constants, and ΔC_0 is the mean-field jump in specific heat. All other symbols have the same meanings as above. Equation (18) is valid in the limits of $b\ll 1$ and $b^2\ln a\chi\ll 1$. Therefore, fluctuation effects lead to modification of the Landau coefficients by logarithmic factors and to a singular term proportional to the jump in heat capacity. The last term remains nonzero in the high-temperature phase. Adding terms for quadratic coupling in strain and differentiating Eq. (18) gives the following expression for the anomalous elastic constant with logarithmic corrections:

$$\begin{aligned}\Delta C_{\text{LC}}^{E=0}&=\tfrac{1}{3}\Delta C_{\text{MF}}^{E=0}\left[\left[1+3b\ \ln\frac{t_0}{t}\right]^{1/3}-1\right],\quad t>0\\&=\tfrac{1}{3}\Delta C_{\text{MF}}^{E=0}\left[4\left[1+3b\ \ln\frac{t_0}{2|t|}\right]^{1/3}-1\right],\quad t<0\ ,\end{aligned} \tag{19}$$

where $\Delta C_{\text{MF}}^{E=0}$ is the mean-field jump in elastic constant at T_c and $t_0=a/t$. For $b\ln(t_0/t)\ll 1$, Eq. (19) can be expanded to yield

$$\Delta C_{\mathrm{LC}}^{E=0} = -\tfrac{2}{3}\Delta C_{\mathrm{MF}}^{E=0} b \ln\left[\left(\frac{A_0}{a}t\right)^{1/2}\right], \quad t>0$$
$$= \Delta C_{\mathrm{MF}}^{E=0} - \tfrac{8}{3}\Delta C_{\mathrm{MF}}^{E=0} b \ln\left[\left(\frac{2A_0}{a}t\right)^{1/2}\right], \quad t<0 . \tag{20}$$

Since $\Delta C_{\mathrm{MF}}^{E=0}$ is negative and t less than one, Eq. (20) predicts, in addition to the mean-field anomalies, a logarithmic decrease of the velocity of sound in both phases near T_c.

Figure 9 shows the anomalous part of the elastic constant along the a axis calculated from the ISBS data by subtracting the rather constant background shown in Fig. 6. The solid line represents the best fit of mean-field theory with the calculated order parameter relaxation time and T_n determined earlier. Deviation from mean-field theory is very apparent in both phases, with the temperature range in which corrections are seen being larger in the symmetric phase. In fact such corrections are present for all three axes and are most apparent in the symmetric phase since no anomalies are predicted by mean-field theory.

Figure 10 plots the corrections to mean-field theory against $\ln|T-T_c|$. In the symmetric phase, linear dependences are obtained for all three axes for a range of temperature of over 50 K. For the low-temperature phase, due to the uncertainty in determining background values in the b and c axes, analysis is carried out only for the a axis. For this axis, logarithmic corrections are apparent in the LT phase over a temperature range of 10 K. Obvious bending of the data occurs near the high-temperature end of the corrections. This behavior has been discussed in terms of a dipolar Ising crossover.[10] However, since the bending occurs nearly 50 K away from T_c, the expansion in Eq. (20) may no longer be valid.

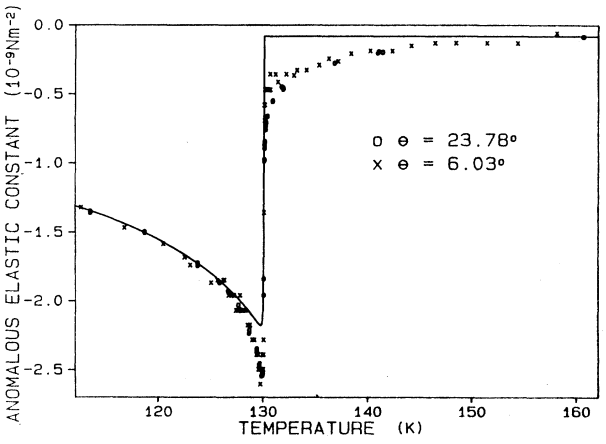

FIG. 9. Acoustic anomalies: Deviation from mean-field behavior in TSCC. Longitudinal anomalous elastic constant values along the a axis, measured with two scattering angles, are shown on an expanded temperature scale. The solid line is the mean-field prediction (for 23.7° scattering angle) as determined by low-temperature data. Deviations are evident for an extended range of temperature above the transition and for a smaller range below the transition. Similar behavior is observed along the c axis.

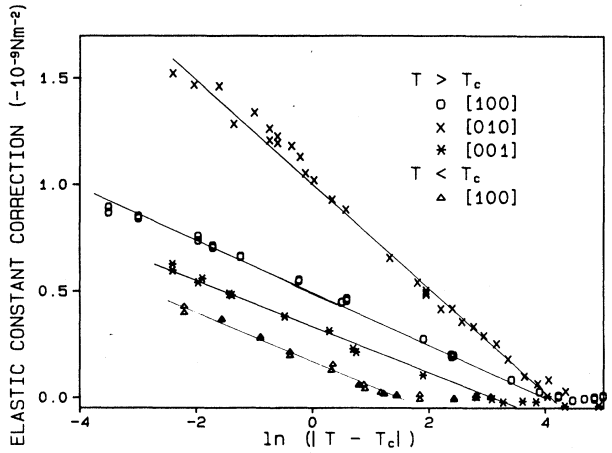

FIG. 10. Elastic constant corrections vs T on a logarithmic temperature scale. Deviations of the anomalous elastic constants from mean-field predictions are calculated by subtracting the mean-field predictions as shown in Fig. 9 from the anomalous elastic constant values measured. Results from all principle axes are shown for the HT phase. The corrections are found to be linear on a logarithmic scale for a temperature range of about 60 k above T_c. For the LT phase, results for the a axis are shown and linear behavior is found for a much smaller range of about 5 K.

Equation (20) offers several predictions that can be compared with experimental data obtained in both phases. As can be seen in Fig. 10, the factor of 4 difference in slopes between the HT and LT phase corrections predicted by Eq. (20) was not observed. The observed slopes are essentially the same in both phases. Equation (20) also predicts a difference between the two phases of a factor of $\sqrt{2}$ for the temperature ranges in which logarithmic corrections are significant. The observed factor is close to 5 instead. Concerning the unusually large dipolar region in TSCC, the prediction is that the dipolar region should increase with the Curie constant and T_c. For TGS, which has a much higher Curie constant and transition temperature, corrections to mean-field behavior are not at all obvious.[26] The constants a and b are functions of the polarization correlation lengths which are not expected to be very different between TSCC and TGS. Therefore Eq. (20) does not offer a quantitative description for TSCC. One obvious shortcoming of applying Eq. (20) to TSCC is the absence of the important sixth-order term. Therefore, theories developed for tricriticality may be more appropriate. Analysis based on phenomenological arguments and tricriticality predicts a factor of 4 between the two temperature ranges[10] in very good agreement to experiment.

D. Acoustic dispersion

To account for order parameter relaxation dynamics, the acoustic velocity anomalies are given by the real part of Eq. (11) with χ_0 replaced by

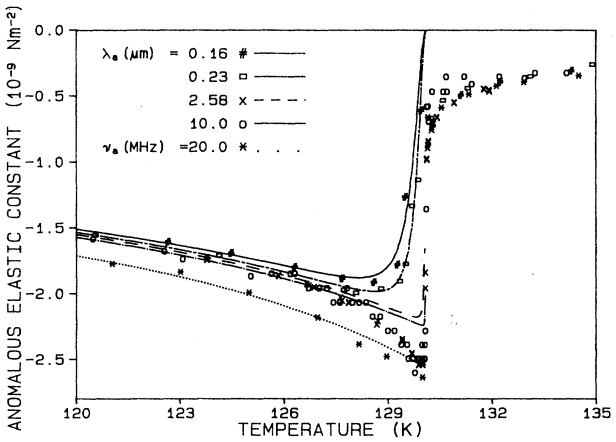

FIG. 11. Dispersion of acoustic velocity anomalies along the a axis of TSCC. ISBS data were compared to ultrasonic (Ref. 14) and Brillouin scattering (Refs. 15 and 10) data to reveal the Debye relaxation dynamics of the order parameter. Due to discrepancies in background velocities and transition temperatures among reported works, all velocities were normalized against their values at T_c+60 K, and temperature axes were translated to obtain a common value of T_c at 132.21 K. Solid lines are mean-field theoretical fits calculated according to Eqs. (21) and (13) with T_c and T_n held at previously determined values and $Q^2\sqrt{A_0C}$ and τ_0 taken as adjustable parameters. The fits yielded $\tau_0=5.5\times10^{-12}$ s K. Ultrasonic data give a larger velocity jump that is not accounted for by the polarization dynamics.

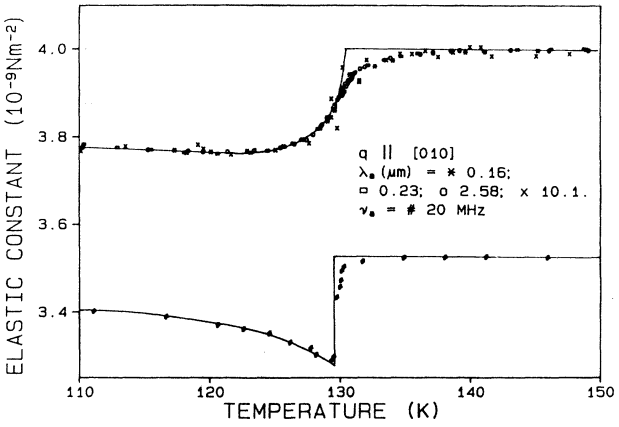

FIG. 12. Dispersion of acoustic velocity anomaly along polar b axis of TSCC. ISBS data were compared to ultrasonic and Brillouin-scattering data (see Fig. 11 for other details.) As a result of the depolarization field along the polar axis, the sharp features seen along the transverse directions are smoothed out together with all the dispersion effects. The solid line on top is a fit of data according to Eq. (17). Ultrasonic data showed a markedly different temperature dependence with a sharp feature near T_c.

$$\chi(\mathbf{q},\omega_a)=\frac{\chi(\mathbf{q})}{1-i\omega_a\tau}\ , \tag{21}$$

where $\tau=\tau_0/(T_c-T)$. The velocity behavior near T_c therefore becomes frequency dependent. As can be seen in Fig. 11, Eq. (21) with elementary relaxation time $\tau_0=5.5\times10^{-12}$ describes well the dispersive behavior from 0.3 to 30 GHz along the a axis, exclusive of logarithmic corrections which are not included in Eq. (11). The feature to note is that the acoustic anomaly at low frequencies, i.e., long acoustic wavelengths, is very sharp, while at the shortest two acoustic wavelengths corresponding to Brillouin-scattering experiments with 90° and backscattering angles, the anomaly is rounded out as a result of $\omega_a\tau$ approaching unity $\sim0.5°$ from T_c. The consequent rounding of the acoustic anomaly probably has prevented clear observation of logarithmic corrections in the LT phase in Brillouin-scattering experiments. With the ISBS scattering angles, these corrections are readily observed. They should also be observable in ultrasonic experiments, but their elucidation would require a higher density of experimental data points than available in the published results. The 20-MHz values shown can be fit adequately by mean-field results, as indicated in Fig. 11.

The value of the elementary relaxation time τ_0 in TSCC is short compared to that in other ferroelectrics such as KDP. However, the microscopic motion involved is quite different than the hydrogen tunneling and associated motions in the KDP family. NMR studies[29] indicate that the relaxation is associated with the motion of the bridging methyl group on the sarcosine molecules.

For the b axis, no dispersion effects can be seen over the three decades of frequency sampled by ISBS and Brillouin scattering. See Fig. 12. Rounding of the anomalies near T_c due to the depolarization field obscures dispersion effects which are small because of the low value of τ_0. At ultrasonic frequencies, the anomaly along the polar axis shows markedly different behavior (see Fig. 12). The sharp behavior is probably caused by energy relaxation[30] (i.e., population relaxation) of the polarization mode. The energy relaxation time is generally much slower than the polarization relaxation time. The acoustic anomaly due to the energy relaxation process is, of course, not influenced by the depolarization field. Such an anomaly is predicted to be proportional to the anomalous heat capacity which is itself logarithmic.[11] The two relaxation times are not directly related to each other. Thus earlier reports[15] connecting the anomalies found in MHz and GHz regimes are not supported.

V. CONCLUSIONS

Longitudinal acoustic anomalies in 0.3- and 2-GHz regions have been measured in TSCC along all three principle axes. Their behaviors have been discussed in terms of mean-field and fluctuational theories. The following conclusions are reached from ISBS data. (1) Logarithmic corrections to mean-field behavior are observed along all three principle directions in the symmetric phase and along the directions transverse to the polar axis in the low-temperature phase. (2) The dispersion observed along the a ([100]) and c ([001]) axes can be explained by a Debye relaxation model for the order-parameter dynamics, with elementary relaxation time $\tau_0=5.5\pm0.2\times10^{-12}$ s K. (3) Along the polar axis b ([010]) no

dispersion is observed between 0.3–30 GHz while a large dispersion occurs between 0.02–0.3 GHz. The anomalies observed along this axis in the high-frequency region are due to coupling to the order parameter, in spite of the presence of depolarization field. The dispersion observed in the low-frequency region is most likely due to energy relaxation processes to which the strain is coupled. (4) Careful measurements of longitudinal velocities along all three principle axes at different frequencies far from T_c have revealed no dispersive behavior. The erratic velocity behavior observed in an earlier report[16] is, therefore, not reproduced.

Most of the data obtained through ISBS as well as ultrasonics and Brillouin scattering can be explained quantitatively by accounting for proximity to a tricritical point, depolarization field effects, logarithmic corrections to mean-field theory, and order-parameter and energy relaxation dynamics. Fortunately, each of these effects can be isolated rather well by examination of acoustic anomalies along different crystallographic axes and in different frequency regimes. Thus quantitative evaluation has been largely successful. The main theoretical development called for is calculation of logarithmic corrections to MF theory near a tricritical point. Experimental investigation of acoustic behavior in the 20 MHz–1 GHz frequency range should also be carried out to elucidate quantitatively the additional dynamical feature which we have ascribed to energy relaxation effects.

The results we have presented demonstrate the applicability of the ISBS technique to the study of acoustic anomalies in quadratically coupled systems. ISBS offers excellent relative and absolute accuracy for determining acoustic velocity anomalies. Changes in the few percent level can be studied thoroughly with this technique. Its dynamic range represents an important asset in acoustic dispersion studies.

ACKNOWLEDGMENTS

This work was supported in part by National Science Foundation (NSF) Grant No. DMR-8704352. One of us (K.A.N.) thanks the Alfred P. Sloan Foundation for support.

*Present address: Central Research and Development Department, E. I. du Pont de Nemours & Co., Wilmington, DE 19898.

[1]T. Ashida, S. Bando, and M. Kakudo, Acta Crystallogr. Sect. B **28**, 1560 (1972).

[2]F. Engelke, D. Michel, and F. Pille, Phys. Status Solidi B **125**, 483 (1984).

[3]K. Deguchi, N. Aramaki, E. Nakamura, and K. Tanaka, J. Phys. Soc. Jpn. **52**, 1897 (1983).

[4]T. Chen and G. Schaack, J. Phys. C **17**, 3801 (1984).

[5]J. F. Scott and G. E. Feldkamp, Ferroelectrics **52**, 211 (1983).

[6]Cz. Pawlaczyk, H.-G. Unruh, and J. Petzelt, Phys. Status Solidi B **136**, 435 (1986).

[7]A. I. Larkin and D. E. Khmelnitskii, Zh. Eksp. Teor. Fiz. **56**, 2087 (1969) [Sov. Phys.—JEPT **29**, 1123 (1969)].

[8]A. Aharony, Phys. Rev. B **8**, 3363 (1973); R. A. Cowley, *ibid.* **13**, 4877 (1976).

[9]E. Sandvold and E. Courtens, Phys. Rev. B **27**, 5660 (1983).

[10]G. A. Smolensky, I. G. Siny, A. K. Tagantsev, S. D. Prokhorova, V. D. Mikvabiya, and W. Windsch, Pis'ma Zh. Eksp. Teor. Fiz. **39**, 307 (1984) [JETP Lett. **39**, 368 (1984)]; G. A. Smolensky, I. G. Siny, A. K. Tagantsev, S. D. Prokhorova, and W. Windsch, Ferroelectrics **64**, 221 (1985).

[11]A. Lopez-Echarri and M. J. Tello, J. Phys. D **14**, 71 (1981).

[12]S. D. Prokhorova, G. A. Smolensky, I. G. Siny, E. G. Kuzminov, V. D. Mikvabia, and H. Arndt, Ferroelectrics **25**, 629 (1980).

[13]L. C. Brunnel, J. C. Bureau, S. Wartewig, and W. Windsch, Chem. Phys. Lett. **72**, 119 (1980).

[14]S. Sorge, U. Straube, and N. R. Ivanov, Phys. Status Solidi A **65**, 189 (1981).

[15]T. Hikita, P. Schnackenberg, and V. H. Schmidt, Phys. Rev. B **31**, 299 (1985).

[16]J. T. Wang and V. H. Schmidt, Phys. Rev. B **34**, 416 (1986).

[17]M. R. Farrar, L.-T. Cheng, Y.-X. Yan, and K. A. Nelson, IEEE J. Quantum Electron. **QE-22**, 1453 (1986); L.-T. Cheng and K. A. Nelson, Phys. Rev. B **37**, 3603 (1988).

[18]Y.-X. Yan, L.-T. Cheng, and K. A. Nelson, J. Chem. Phys. **88**, 6477 (1988).

[19]Th. Nattermann, Phys. Status Solidi B **85**, 291 (1978).

[20]K. A. Nelson, R. J. D. Miller, D. R. Lutz, and M. D. Fayer, J. Appl. Phys. **53**, 1144 (1982).

[21]Y.-X. Yan and K. A. Nelson, J. Chem. Phys. **87**, 6240 (1987); **87**, 6257 (1987).

[22]See, for example, W. H. Press, B. P. Flannery, S. A. Teukolsky, and W. T. Vetterling, *Numerical Recipes* (Cambridge University Press, Cambridge, 1986).

[23]L. D. Landau and E. M. Lifthitz, *Statistical Physics,* Eng. transl. (Pergamon, Oxford, 1976).

[24]J. C. Slonczewski and H. Thomas, Phys. Rev. B **1**, 3599 (1970).

[25]L. D. Landau and E. M. Lifshitz, *Electrodynamics of Continuous Media,* Eng. transl. (Pergamon, Oxford, 1957).

[26]T. Yagi, M. Tokunaga, and I. Tatsuzaki, J. Phys. Soc. Jpn. **40**, 1659 (1976).

[27]M. Tokunaga, Prog. Theor. Phys. **51**, 1002 (1974).

[28]A. P. Levanyuk, Zh. Eksp. Teor. Fiz. **49**, 1304 (1965) [Sov. Phys.—JETP **22**, 901 (1966)].

[29]F. Engelke, D. Michel, and F. Pille, Phys. Status Solidi B **125**, 483 (1984).

[30]K. Kawasaki, Int. J. Magn. **1**, 171 (1971).